ISBN: 978-3-95450-223-3 ISSN: 2673-7000 doi:10.18429/JACoW-NAPAC2019-MOPLM07

SIMULATION OF BEAM ABORTS FOR THE ADVANCED PHOTON SOURCE TO PROBE MATERIAL-DAMAGE LIMITS FOR FUTURE STORAGE RINGS *

M. Borland, J. Dooling, L. Emery, R. R. Lindberg, V. Sajaev, Y.-P. Sun,
ANL, Lemont, IL, USA

Abstract

Damage to tungsten and copper beam dumps has been observed in the Advanced Photon Source (APS), a 7-GeV, third-generation storage ring light source. This issue is expected to be much more severe in the APS Upgrade, owing to doubling of the stored charge and much lower emittance. An experiment was conducted at 6 GeV in the existing APS ring to test several possible dump materials and also assess the accuracy of predictions of beam-induced damage. Prior to the experiments, extensive beam abort simulations were performed with `elegant` to predict thresholds for material damage, dependence on vertical beam size, and even the size of the trenches expected to be created by the beam. This paper presents the simulation methods, simple models for estimating damage, and results. A companion paper in this conference presents experimental results.

INTRODUCTION

Beam dumps are required in storage rings to localize losses and protect sensitive equipment when the beam is aborted due to, e.g., an rf trip. Given that damage to tungsten and copper beam dumps has been observed in the APS [1], there is significant concern about the beam dumps for the APS upgrade (APS-U), since it will have twice the stored current and 100-fold lower horizontal emittance. The decoherence kicker proposed [2] to protect the APS-U swap-out dump is not helpful here, because the entire beam will be lost when the rf trips, for example; this, coupled with the rapid loss of beam following an rf trip, the possibility for kicker failure, and the limited effectiveness of decoherence in inflating the emittance, makes it unavoidable that the whole-beam dumps will be damaged. Doses on the APS-U whole-beam dumps are predicted to be as high as 35 MGy ($35 \times 10^6\,\mathrm{J\,kg^{-1}}$), though they are typically expected to be lower because the losses are usually spread over five dumps.

We realized that it is possible to approach APS-U conditions in APS by adjusting the optics at the dump location to provide reduced horizontal beam size (RHB), reducing the vertical emittance, and running at 6 GeV, since that allows raising the beam current as high as 300 mA. In addition, by moving the beam dump surface close to the closed orbit, we reduce diffusion of the beam from resonances as it spirals inboard during the beam aborts. We selected two alloys, Al6061 and Ti6Al4V as target materials for tests, as reported in [3]. The aluminum alloy was chosen because we have never observed damage to this material in APS, while the titanium alloy was chosen because of its high melting temperature, relatively low Z, and high strength. The target materials were installed on a horizontal-movable scraper in Sector 37 of the APS.

* Work supported by the U.S. Department of Energy, Office of Science, Office of Basic Energy Sciences, under Contract No. DE-AC02-06CH11357.

SIMULATION METHODS

Simulations used the parallel version of `elegant` [4–6]. Because we must predict when and where the beam is lost, we used element-by-element tracking with a calibrated lattice model based on the response matrix fit method [7, 8]. We further included a model of the short-range wakefields [9–12], which has been validated in various experiments [12–14]. The rf systems (16 cavities driven by two klystrons) were included as an `RFMODE` element, which models beam loading, rf feedback [15], and muting of the generator output; these features allow bringing a multi-bunch beam to equilibrium, then tripping the rf systems.

The experiments are described in more detail elsewhere [3]. They involved making a series of fills from a few milliamps to just under 70 mA, limited by unrelated operations issues. For each fill level, the bunch pattern was different, based on operational considerations. The fill pattern details for each case are included in the simulations. Once each fill is created, the scraper is moved to within 2 mm of the closed orbit and a vertical beam bump is created with an amplitude that is unique to each case; this allows unambiguously relating any material damage to the conditions (beam current) prior to the abort. The details of the vertical bumps, including their effect on the vertical emittance through non-zero orbit in vertical sextupoles as well as the attempted nulling of this effect through adjustment of skew quadrupoles, are included in the simulations. However, for reasons still to be understood, the simulations predict significantly larger vertical emittances than measured, by up to a factor of two.

Figure 1 shows information on the timing of the simulated particle losses. The elapsed time relative to the rf trip event for loss of half the beam decreases as the stored current increases, due to beam loading in the rf cavities. The slope is about 50% larger in experiments [3], which suggests that improvements are needed to the rf cavity parameters used in the simulations. The time interval for loss of the central 80 or 90% of the beam also decreases as the stored current increases, for the same reason; the slope is in rough agreement with experiments. This shorter loss interval accentuates the impact of the dose on the dump, since there is less time for thermal diffusion.

ISBN: 978-3-95450-223-3 ISSN: 2673-7000 doi:10.18429/JACoW-NAPAC2019-MOPLM07

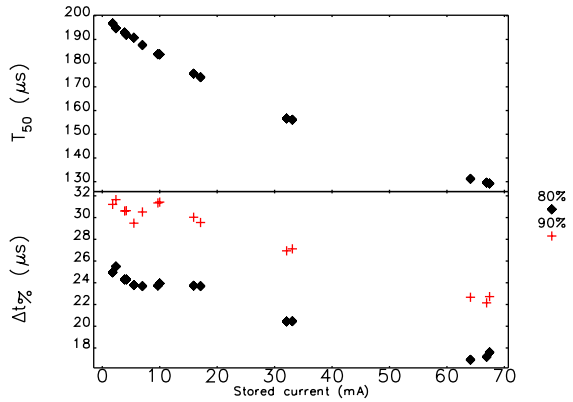

Figure 1: Simulated elapsed time required since rf trip for 50% beam loss (top) and time interval for loss of central 80 or 90% of beam (bottom), as a function of the stored current.

As mentioned, for each case the beam is steered vertically so that the impact with the dump occurs at a unique vertical location. The size of the bump (up to ~5 mm) requires significant orbit distortion in sextupoles, which results in vertical emittance changes, which we tried to control using skew quadrupoles. This wasn't entirely successful, as seen in Fig. 2, where we plot the rms sizes of the beam footprint on the dump as a function of the stored current. The pattern is different for the Al6061 and Ti6Al4V targets because the former (latter) requires a positive (negative) bump that generally increased in amplitude for higher stored current. There is one aberrant point for Al6061, where a small bump amplitude was used for high current, giving smaller vertical emittance. A simple estimate using TAPAs [16] based on data in [17] gives a maximum dose of about 20 MGy.

Note that the rms footprint size in the horizontal is significantly less than the rms size of the stored beam at the dump location, since the beam is intercepted piece-by-piece as it spirals in. The area of each piece is larger when the current is higher, because the energy loss per turn is faster due to voltage induced in the rf cavities, but the horizontal footprint is still less than the ~ 110 μm rms beam size.

THERMAL DIFFUSION

As indicated above, the beam loss takes place over 5 to 9 turns, depending on the initial stored current. This provides time for thermal diffusion, which can reduce the chance that material will be melted. This process is governed by the diffusion equation

$$\frac{\partial}{\partial t}\Theta(\mathbf{r},t) = \alpha\nabla^2\Theta(\mathbf{r},t) + S(\mathbf{r},t), \qquad (1)$$

where Θ is the temperature, α the thermal diffusivity, and S the heat distribution. From simple inspection, we see that the time and length scales of diffusion are related by $\alpha t_{diff} \sim L^2_{diff}$. Solution of the diffusion equation for a radially-gaussian source $S \sim \exp\left[-r^2/(2\sigma^2)\right]\delta(t)$ confirms this, showing that the temperature increase is reduced by the factor $\sigma^2/(\sigma^2 + \alpha t_{diff})$. The effect of diffusion over a time Δt can thus be approximated by convolving the distribution computed in the absence of diffusion with a radial gaussian with $\sigma_{diff} = \sqrt{\alpha\Delta t}$.

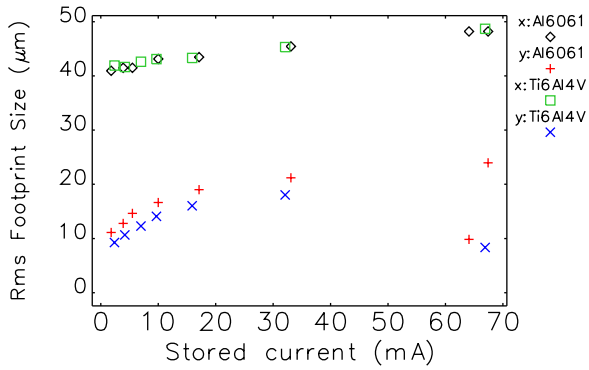

Figure 2: Simulated horizontal (x) and vertical (y) rms footprint sizes on the dump as a function of stored current, delineated by the type of material.

ESTIMATION OF MATERIAL DAMAGE

While estimation of material damage is possible using the dose computed from the rms footprint size, the heat capacity, and the melting temperature [1], this oversimplifies the beam distribution and neglects thermal diffusion. The former can be included by pixelating the dump surface to get a dose map, while the latter can be included approximately using the thermal diffusivity, as just described. We marry these approaches by convolving the dose map with a 2d gaussian distribution having $\sigma_{x,y} = \sigma_{diff}$ The pixel size is taken as $\sigma_{diff}/6$ to ensure adequate resolution. We used the 80- and 90-percent loss intervals, shown in Fig. 1 for Δt. However, the results are very similar so we show only the 80% loss computations.

Using material properties listed in Table 1, we computed the dose for each pixel $\hat{D}_{ij} = (Q_{ij}d)/(\Delta x\Delta y)$, where Q_{ij} is the charge impacting the pixel of size Δx by Δy, and d is the specific dose, computed using data from the NIST ESTAR database [17]. We convolved $\hat{D}_{ij}$ with the thermal-diffusion function, giving the effective dose map D_{ij}. Using the specific heat capacity C_p, we compared D_{ij} to the dose required to reach the melting point and liquify the metal, i.e., $\Delta D_m = (T_m - 298)C_p + \Delta H_m$, where ΔH_m is the heat of melting. Note that we've (incorrectly) assumed that all properties are temperature-independent.

Figures 3 and 4 show the effective dose map for two of the highest-current cases for Al6061 and Ti6Al4V, corresponding to the two points with vertical footprint size of ~9 μm on the right-hand-side of Fig. 2. To understand the impact of thermal diffusion, note that the raw dose maps show a peak dose in Al6061 that is within 20% of that in Ti6Al4V. However, with diffusion included, the peak effective dose in Ti6Al4V is 4 times higher than in Al6061, owing to the

ISBN: 978-3-95450-223-3 ISSN: 2673-7000 doi:10.18429/JACoW-NAPAC2019-MOPLM07

Table 1: Material properties used in temperature-rise and melting estimates. Values for ΔH_m are for pure aluminium and titanium.

material	d $\frac{\text{Gy mm}^2}{\text{nC}}$	α $\frac{\mu\text{m}^2}{\mu\text{s}}$	C_p Gy K^{-1}	T_{melt} K	ΔH_m kJ kg^{-1}
Al6061	215.3	64	910	853	397
Ti6Al4V	202.0	3	561	1873	295

much more rapid diffusion of heat in the latter. This does not prevent melting, however, because Al6061 has a much lower melting temperature, even though it has a much higher heat capacity.

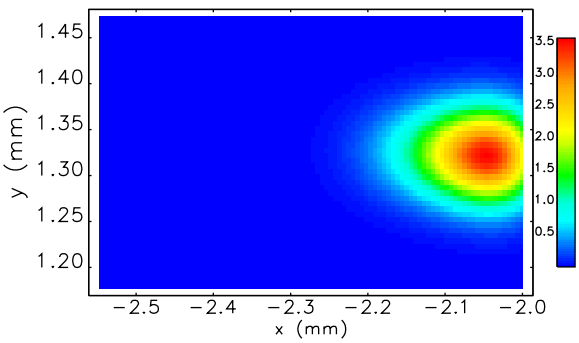

Figure 3: Predicted effective dose map (MGy) for 64-mA strike on Al6061 with small vertical footprint, after convolution with diffusion effect.

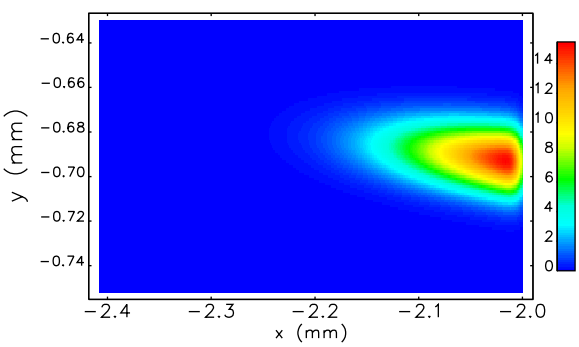

Figure 4: Predicted effective dose map (MGy) for 67-mA strike on Ti6Al4V with small vertical footprint, after convolution with diffusion effect.

Figure 5 shows the predicted area of the dump that is liquefied by the beam impact. We see that in Al6061, the onset of liquefaction occurs for stored current above ∼16 mA, while for Ti6Al4V, the threshold is about 7 mA. The explanation is that, in spite of its lower melting temperature, Al6061 has much higher thermal diffusivity than Ti6Al4V which, combined with the fact that the beam is scraped away over several tens of microseconds, delays the onset of liquefaction. Once Al6061 passes the melting threshold, however, the area liquefied is larger owing, again, to thermal diffusion.

These results present a somewhat complex choice: the melting threshold in Al6061 is about three-fold higher than for Ti6Al4V, but for high current, the area of Al6061 melted is larger and appears to be increasing rapidly. Since the maximum dose for APS-U is expected to be higher than reached in our experiments, this may be relevant if the predictions are reliable. One issue with Ti6Al4V is that it becomes activated when struck by an electron beam, which may pose problems for maintenance and disposal.

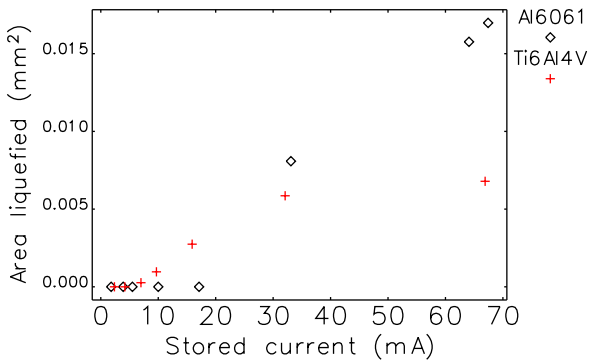

Figure 5: Predicted area liquefied as a function of the stored current prior to the beam abort.

CONCLUSIONS

Because of the high energy, high current, and ultra-low emittance, APS-U beam dumps are expected to be damaged by the beam, with expected doses of several tens of MGy. We recently performed experiments at APS to model such conditions by reducing the horizontal and vertical beam sizes at the location of a scraper equipped with two targets, one of Al6061 and one of Ti6Al4V. We used particle tracking to model these experiments in some detail, including transient beam-loading in the rf cavities following an rf trip. The transverse loss map from these simulations was used together with an approximate treatment of thermal diffusion to estimate the onset of melting as a function of current, as well as the size of the melt region. The former seem in reasonable agreement with the experiments, which are described elsewhere in these proceedings [3].

ACKNOWLEDGMENTS

This work used the Blues and Bebop clusters at Argonne National Laboratory.

ISBN: 978-3-95450-223-3 ISSN: 2673-7000 doi:10.18429/JACoW-NAPAC2019-MOPLM07

REFERENCES

[1] J. C. Dooling, M. Borland, Y. C. Chae, and R. Lindberg, "Energy deposition in the Sector 37 scraper of the Advanced Photon Source Storage ring," in *Proc. PAC'13*, pp. 1361–1363, 2014.

[2] M. Borland, J. Dooling, R. Lindberg, V. Sajaev, and A. Xiao, "Using decoherence to prevent damage to the swap-out dump for the APS Upgrade," in *Proc. IPAC'18*, pp. 1494–1497, 2018.

[3] J. C. Dooling *et al.*, "Studies of beam dumps in candidate horizontal collimator materials for the Advanced Photon Source Upgrade storage ring," presented at *NAPAC'19*, p. MOPLM14, 2019, this conference.

[4] M. Borland, "elegant: A Flexible SDDS-Compliant Code for Accelerator Simulation," Tech. Rep. ANL/APS LS-287, Advanced Photon Source, September 2000.

[5] Y. Wang and M. Borland, "Pelegant: A Parallel Accelerator Simulation Code for Electron Generation and Tracking," *AIP Conf. Proc.*, vol. 877, p. 241, 2006.

[6] M. Borland, "Improvements in Modeling of Collective Effects in ELEGANT," in *Proc. IPAC'15*, pp. 549–552, 2015.

[7] J. Safranek, "Experimental determination of storage ring optics using orbit response measurements," *NIM A*, vol. 388, 1997.

[8] V. Sajaev and L. Emery, "Determination and correction of the linear lattice of the APS storage ring," in *Proc. EPAC 2002*, pp. 742–744, 2002.

[9] Y.-C. Chae, K. Harkay, and X. Sun, "Longitudinal coupling impedance of the APS storage ring," in *Proc. PAC'03*, pp. 3014–3016, 2003.

[10] Y.-C. Chae, "The impedance database and its application to the APS storage ring," in *Proc. PAC'03*, p. 3017, 2003.

[11] Y.-C. Chae, Y. Wang, and A. Xiao, "Impedance database ii for the advanced photon source storage ring," in *Proc. PAC'07*, Albuquerque, NM, pp. 4336–4338, 2007.

[12] R. R. Lindberg and A. Blednykh, "Modeling of impedance effects for the APS-MBA upgrade," in *Proc. IPAC'15*, pp. 1825–1827, 2015.

[13] V. Sajaev, M. Borland, Y.-C. Chae, and L. Emery, "Experimental verification of single-bunch accmulation limit dependence on impedance at the APS," in *Proc. PAC'13*, pp. 405–407, 2013.

[14] V. Sajaev, R. Lindberg, M. Borland, and S. Shin, "Simulations and measurements of the impact of collective effects on dynamic aperture," *Phys. Rev. Accel. Beams*, vol. 22, p. 032802, Mar 2019.

[15] T. Berenc and M. Borland, "Modeling RF Feedback in Elegant for Bunch-Lengthening Studies for the APS," in *Proc. IPAC'15*, pp. 540–542, 2015.

[16] M. Borland, "Android Application for Accelerator Physics and Engineering Calculations," in *Proc. NAPAC'13*, pp. 1364–1366, 2013.

[17] https://physics.nist.gov/PhysRefData/Star/Text/ESTAR.html